(2) LEVEL II

(6) OBLIQUE WATER ENTRY AND EXIT OF A FULLY VENTILATED FOIL

by

(10) D. P. Wang

Prepared for

David W. Taylor

Naval Ship Research and Development Center

Wang (D. P.) Arlington, VA

(15) N00167-77-M-8075

This work was supported by the Naval Material Command (0333), Program Element 62543N, Task Area ZF-43-421-001, administered by the David W. Taylor Naval Ship Research and Development Center, Work Unit 1500-200.

(12) 44p.

(11) July 1977

AD A065007

LB

OBLIQUE WATER ENTRY AND EXIT OF A FULLY VENTILATED FOIL

by

D. P. Wang

Suite 54, 1121 Arlington Boulevard

Arlington, Virginia 22209

SUMMARY

The oblique entry of a two-dimensional, fully ventilated foil into a horizontal layer of water of arbitrary thickness is considered. When the thickness of the layer is finite, exit of the foil from the layer is studied. The present work is an extension of a previous one [1], in which only vertical entry and exit of the foil were considered. The consideration of oblique entry makes the present solution useful in studying not only the advance ratio effect on a partially submerged supercavitating propeller but also many other problems, such as the high-speed water entry and exit of a wing or a control surface, the operation of a high-speed hydrofoil in a high sea state. The results obtained in this work indicate that the force and moment coefficients of a foil decrease as the advance ratio is reduced.

1. INTRODUCTION

In a previous paper [1], the present author used a linearized flow model to study the flow characteristics around a partially submerged supercavitating propeller operating in the vicinity of an ocean surface. The model was fashioned after the blade element theory for the conventional marine propeller. When the effects of the neighboring blades and of gravity were ignored, the flow resembled that of the entry into and exit from a horizontal layer of water of finite thickness by a two-dimensional, fully ventilated foil in a gravity-free space. The circular-arc length traveled in the ocean by the leading edge of the blade element was taken as the thickness of the layer. The upper and lower surfaces of the layer, which represented the ocean surface, were assumed to be exposed to atmospheric pressure. The foil, which represented the blade element, entered vertically into the upper free surface of the layer and exited from its lower free surface. When moving in the water, the foil was allowed to have small, unsteady deformations, so that the theory could be applied to hydroelastic studies.

In studying the problem, the flow motion considered in [1] was divided into three different phases: the initial entry, the complete entry, and the exit. The flow motion is defined as being in the initial entry phase when the foil is only partially submerged, in the complete entry phase when the foil is completely submerged, and in the exit phase when the leading edge of the foil pierces through the lower free surface of the layer. For the exit phase, the pressure distribution on the foil was explicitly determined;

for the other two phases, however, it was determined analytically except for a function of the time factor. The determination of the function depended on the solution of a system of integral equations. The integral equations, which governed the flow speed on the cavity walls, were produced as a consequence, when the role played by the time factor in solving the flow velocity was reduced from an explicit variable to a parameter. For the special case when the thickness of the layer became infinite and the flow was in its initial entry phase, solutions for arbitrary foil deformations were obtained in [illegible]ies forms. For other cases, numerical methods were devised to solve the integral equations.

The results obtained in [1] show that the rate of increase in the loading on the foil is most rapid during the initial entry and that the loading almost reaches its maximum at the end of this phase. During the same phase, the influence of the thickness of the layer on the foil loading is small and may be neglected for most cases. This finding may become very useful when the structural design of a propeller blade is considered.

The theory developed in [1], however, did not consider the advance ratio effect, which is known to have some influence on the thrust and torque coefficients of the partially submerged propeller. To consider the advance ratio effect, the foil should enter the horizontal layer of water obliquely, instead of vertically as in [1]. The main purpose of the present paper is to consider such an effect: that is, to study the oblique entry and exit of a fully ventilated foil from a layer of water of finite thickness. The limiting case when the thickness of the layer becomes infinite is

also considered.

Numerical results for a flat plate foil and for circular-arc foils are obtained. They indicate that, when the angle of attack measured from the entering path of a foil remains constant, the force and moment coefficients of the foil decrease as the advance ratio is reduced.

2. DESCRIPTION OF THE PROBLEM

When the blade of a partially submerged supercavitating propeller enters an ocean surface, the flow is expected to separate from the leading edge of the blade, forming on the suction side a cavity that vents to the atmosphere. When the flow model described in [1] is adopted and the advance ratio effect considered, the corresponding flow becomes that of the oblique entry of a two-dimensional, fully ventilated foil into a horizontal layer of water of finite thickness, as shown in Fig. 1. The upper and lower surfaces of the layer are assumed to be exposed to the atmospheric pressure p_a. The foil enters the upper free surface and exits from the lower one with a constant velocity U, which is assumed to be large enough to cause the flow around the foil to become separated but not so large as to render the incompressible and inviscid approximations invalid. In this work, the flow separation is assumed to occur immediately after the entry of the leading edge, and the pressure inside the cavity to be always equal to p_a.

In Fig. 1, the leading edge of the foil is denoted by B, and the trailing edge by T. The cavity walls are represented by the curves BC and TA. C and A are the intersectional points where the cavity walls and the upper free surface of the layer meet.

When the chord length of the foil, ℓ, is taken as the charac-

teristic length, the non-dimensional thickness of the layer is denoted by h. The entering speed U and time ℓ/U are taken as the characteristic speed and time respectively. The non-dimensional pressure p is defined by

$$p = (\tilde{p}-p_a)/(\tfrac{1}{2}\rho U^2), \tag{1}$$

where $\tilde{p}$ is the dimensional pressure and ρ the density of water. Based on these characteristic quantities, physical parameters of the present problem can be made into non-dimensional forms, which are used in the following analysis.

For reference, a Cartesian coordinate system (x,y) is chosen; the x-axis lies on the original undisturbed upper free surface of the layer, and the y-axis points vertically upwards. At time t=0, the leading edge of the foil is assumed to touch the upper free surface at the origin of the x-y axes. The angle between the velocity U and the x-axis is denoted by $\gamma\pi$, as shown in Fig. 1. Without loss of generality, it may be assumed that $0 < \gamma \leq \frac{1}{2}$. When the advance ratio, λ, of a blade element is defined as the ratio of the propeller's advance speed to its circumferential speed at the location where the blade element is situated, λ may be expressed as

$$\lambda = \tan(\tfrac{1}{2}-\gamma)\pi. \tag{2}$$

Suppose during its motion in the water the foil is performing small (say, of the order of ε), unsteady motions about its entering path, and suppose the percentage change in the chord length of the foil is less than the order of ε. Then, to the first order in ε, the locations of points on the foil surface at any t may be described by the equation

$$n = \varepsilon g(s,t) \quad \text{for} \quad t-1 \leq s \leq t. \tag{3}$$

In (3), s is the distance measured from the origin of the x-y axes along the entering path, n the distance measured normal to s, as indicated in Fig. 1, and g(s,t) is assumed to be given. ε is so small that the conventional linearized approximation used in solving an inviscid free surface flow problem for small disturbances may be used.

Since the flow is considered incompressible and inviscid, a velocity potential $\phi(x,y,t)$ may be used to describe the motion of the water. Consequently, when the effect of gravity is neglected, the linearized equation of motion becomes

$$\phi_t + p/2 = 0. \tag{4}$$

The constant pressure condition p=0 on the free surface may now be stated as

$$\phi_t = 0. \tag{5}$$

Consistent with the adopted linearization process, this already linearized boundary condition need not be applied to the actual locations of the free surfaces. Instead, it may be applied to the planes y=0 and y=-h, and to the portions of the entering path that correspond to the cavity walls as $\varepsilon \to 0$.

On the wetted side of the foil, the linearized boundary condition is

$$\phi_n = \varepsilon g_t(s,t), \tag{6}$$

which is applied to the portion of the entering path corresponding to the wetted side of the foil as $\varepsilon \to 0$. At $x=\pm\infty$, which are denoted by points D and E in Fig. 1, it is required that

$$\phi_x = \phi_y = 0 \quad \text{for} \quad t \geq 0. \tag{7}$$

The boundaries to which the linearized boundary conditions are applied define the linearized flow field. Since the layer of water is assumed to be originally motionless, the initial condition may be stated as

$$\phi = 0 \tag{8}$$

in the entire flow field.

As explained in [1], it is possible to express the boundary condition (5) as

$$\phi_x = 0 \tag{9}$$

on the free surfaces y=0 and y=-h, and as

$$\phi_s = q(s) \tag{10}$$

on the cavity walls where n=0. In (10), q(s), the speed function on the cavity walls, is not yet known, but it will be determined in the process of solving the problem. The advantage of replacing the free surface boundary condition (5) by (9) and (10) is that the variable t now acts merely as a parameter in solving the flow velocity.

3. SOLUTIONS

The boundary conditions (6), (7), (9) and (10) form a typical boundary-value problem, whose solution determines the velocity field that includes the unknown speed function q(s). To solve the present problem, the same method of solution used in [1] is adopted here. The flow motion is divided into three different phases: the initial entry, the complete entry, and the exit. The solution to each phase is sought separately.

To find the solutions for the initial and the complete entry phases, the linearized flow field is mapped onto the upper-half of a parametric ζ-plane for a given t, as shown in Fig. 2, where the images of points A, B, C, D, E and T are labelled accordingly: point A is mapped to the origin of the ζ-plane, B to (b,0), C to (c,0), D to the point of infinity, E to (-1,0) and T to (τ,0). The mapping function may be expressed as

$$\frac{\partial z}{\partial \zeta} = -\frac{h}{\pi}\zeta^{-\gamma}(\zeta-b)(\zeta-c)^{\gamma-1}(\zeta+1)^{-1}, \tag{11}$$

where $z=x+iy$ and $\zeta=\xi+i\eta$. In (11), the branch cut is chosen to lie between $\zeta=0$ and $\zeta=c$ with $0 \leq \mathrm{Arg}(\zeta) < 2\pi$ and $0 \leq \mathrm{Arg}(\zeta-c) < 2\pi$. It can be shown from (11) that

$$c = (1+b)^{\frac{1}{1-\gamma}}-1 \tag{12}$$

and that b as a function of t is governed by the equation,

$$\pi t/h = \int_0^1 \mu^{-\gamma}(1-\mu)(c/b-\mu)^{\gamma-1}(1/b+\mu)^{-1}d\mu. \tag{13}$$

The integral shown in (13) can be expressed in terms of a hypergeometric function of two variables; however, it is more convenient for future applications to express the relationship between b and t numerically. The results for several values of λ are shown graphically in Fig. 3. It should be noted that the correspondence of b=0 with t=0 and of b=∞ with $t=h\csc\gamma\pi$ can each be shown analytically.

On the boundary $0 \leq \xi \leq c$, the dependence of s on ξ and t may be expressed in an integral form as

$$\pi s/h = \int_0^{\xi} \nu^{-\gamma}(b-\nu)(c-\nu)^{\gamma-1}(1+\nu)^{-1}d\nu. \tag{14}$$

Obviously, s has only one extremum in the region $0 \leq \xi \leq c$. This

occurs at $\xi=b$, at which $s=t$. As ξ increases from 0 to b, s increases monotonically from 0 to t; as ξ further increases from b to c, s decreases monotonically from t to 0.

Initial Entry

This phase of motion occurs during the time interval $0 \leq t \leq 1$, in which the trailing edge of the foil has not yet become submerged. Consequently, only one cavity wall is generated. This is located on the suction side of the foil and is described in Fig. 1 as BC.

Suppose the unknown speed function q(s) on the cavity wall BC is designated by $q_1(s)$. By solving the boundary-value problem (cf. [1]), the complex velocity w(z,t), which satisfies the finite pressure condition at point A and C and the ½-root type of singularity in pressure at point B, becomes

$$w = \frac{1}{\pi i} \frac{(\zeta-c)^{1-\gamma}}{\zeta^{\frac{1}{2}-\gamma}(\zeta-b)^{\frac{1}{2}}} \{\int_0^b g_t(s,t)+\int_b^c q_1(s)\} \frac{\xi^{\frac{1}{2}-\gamma}|\xi-b|^{\frac{1}{2}}}{(c-\xi)^{1-\gamma}} \frac{d\xi}{\xi-\zeta}, \qquad (15)$$

where $q_1(s)$ is the solution of the integral equation

$$\int_0^t [g_t(s,t)+q_1(s)] \left(\frac{\xi}{|\xi-b|}\right)^{\frac{1}{2}} ds = 0. \qquad (16)$$

In the above expressions, ζ is regarded as a function of z and t, ξ a function of s and t, and the function $(\zeta-b)^{\frac{1}{2}}$ is restricted to the branch specified by $0 \leq \mathrm{Arg}(\zeta-b) < 2\pi$. It should be noted that ε, the parameter used to indicate the smallness of the disturbances, has been omitted from (15) and (16). The omission of ε will continue from here onward.

When $g_t(s,t)$ is given, the integral equation (16) determines $q_1(s)$ for $0 \leq s \leq t \leq 1$. However, for the limiting case as $t \to 0$,

$q_1(0)$ can be explicitly determined, and the result is

$$q_1(0) = -Q_0(\gamma) g_t(0,0), \tag{17}$$

where

$$Q_0(\gamma) = \int_0^1 K(\mu)d\mu \Big/ \int_1^{\frac{1}{1-\gamma}} K(\mu)d\mu, \tag{18}$$

and

$$K(\mu) = \mu^{\frac{1}{2}-\gamma} |1-\mu|^{\frac{1}{2}} \left(\frac{1}{1-\gamma} - \mu\right)^{\gamma-1}. \tag{19}$$

Equ. (17) indicates that $q_1(0)$ is independent of h, the thickness of the layer. The function $Q_0(\gamma)$ is plotted in Fig. 4, where the ordinate is Q_0 and the abscissa γ, whose corresponding value of λ is also shown in the figure. With the aid of either (9) or (15), it can be shown that the velocity at point C is always pointing vertically upward, irrespective of the value of γ so long as $0 < \gamma \leq \frac{1}{2}$. The magnitude of this velocity is equal to $Q_0(\gamma) g_t(0,0) \csc\gamma\pi$.

Throughout the initial entry phase, A (i.e., point $\zeta=0$) is the point of contact between the foil and the upper free surface of the layer. The asymptotic behavior of w in the neighborhood of A can be studied from (15). For the case when $0 < \gamma < \frac{1}{2}$,

$$w \sim a_1(t)\zeta^{\gamma-\frac{1}{2}} \quad \text{as } \zeta \to 0, \tag{20}$$

where

$$a_1(t) = \frac{c^{1-\gamma}}{\pi b^{\frac{1}{2}}} e^{-i\gamma\pi} \left\{\int_0^b g_t(s,t) + \int_b^c q_1(s)\right\} \xi^{-\frac{1}{2}-\gamma} |\xi-b|^{\frac{1}{2}} (c-\xi)^{\gamma-1} d\xi. \tag{21}$$

When $\gamma=\frac{1}{2}$, however,

$$w \sim \frac{i}{\pi} g_t(0,t) \ln\zeta \quad \text{as } \zeta \to 0. \tag{22}$$

The pressure distribution on the wetted side of the foil, which lies on the segment $0 \leq \zeta \leq b$, can be derived from (15). The derivation involves the integration of w(z,t) with respect to z

(which produces the complex velocity potential f(z,t)) and the differentiation of f(z,t) with respect to t. The final result may be written as

$$p = \frac{2}{\pi}\left(\frac{c-b}{b}\right)^{1-\gamma} a_2(t)\left(\frac{\zeta}{b-\zeta}\right)^{\frac{1}{2}} + \frac{2}{\pi}\int_0^t g_{tt}(s,t)\,\ln\frac{\left[\sqrt{\zeta(b-\xi)}+\sqrt{\xi(b-\zeta)}\right]^2}{b|\zeta-\xi|}\,ds, \qquad (23)$$

where

$$a_2(t) = \{\int_0^b g_t(s,t) - \int_b^c q_1(s)\}\xi^{\frac{1}{2}-\gamma}|\xi-b|^{-\frac{1}{2}}(c-\xi)^{\gamma-1}d\xi. \qquad (24)$$

The above results form the basis on which numerical calculations for the solution of the initial entry can be made.

Complete Entry

This phase occurs during the time interval $1 < t < h\csc\gamma\pi$, in which both the leading and trailing edges of the foil remain submerged in the water. In this case, a second cavity wall, TA, is generated in addition to the already established BC. The flow configuration has been shown in Fig. 1. Suppose the unknown speed function on BC where $s > 1$ is again designated as $q_1(s)$ and that on TA as $q_2(s)$. Then, the solution for $w(z,t)$ may be written as (cf. [1])

$$w = -\frac{i}{\pi}\left(\frac{\zeta-c}{\zeta}\right)^{1-\gamma}\left(\frac{\zeta-\tau}{\zeta-b}\right)^{\frac{1}{2}}\{\int_0^\tau q_2(s) + \int_\tau^b g_t(s,t) + \int_b^c q_1(s)\}\left(\frac{\xi}{c-\xi}\right)^{1-\gamma}\left|\frac{\xi-b}{\xi-\tau}\right|^{\frac{1}{2}}\frac{d\xi}{\xi-\zeta}, \qquad (25)$$

where τ is the ξ-coordinate of the trailing edge T, whose s-coordinate is (t-1), and the function $(\zeta-\tau)^{\frac{1}{2}}$ is restricted to the branch specified by $0 \leq \mathrm{Arg}(\zeta-\tau) < 2\pi$. The value of τ can be determined from (14) by iterations. The iteration process is a

straightforward one and can be made to converge for any s on the foil or on the cavity walls. This is because s is a monotonically increasing, or decreasing, function of ξ in those ranges.

The unknown speed functions $q_1(s)$ for $1 < s < h\csc\gamma\pi$ and $q_2(s)$ for $0 < s < h\csc\gamma\pi - 1$ are governed by the following two integral equations,

$$\{\int_0^{t-1} q_2(s) + \int_{t-1}^{t} g_t(s,t) + \int_0^{t} q_1(s)\} \frac{1}{|(\xi-\tau)(\xi-b)|^{\frac{1}{2}}} \begin{vmatrix} 1 \\ \\ \xi \end{vmatrix} ds = \begin{vmatrix} 0 \\ \\ 0 \end{vmatrix}. \quad (26)$$

Using the procedures described in the previous section, the pressure p on the foil BT, which lies on the segment $\tau \le \zeta \le b$, can be obtained from (25), and the result may be expressed as

$$p = \frac{2}{\pi}\left(\frac{c-b}{b}\right)^{1-\gamma} a_3(t)\left(\frac{\zeta-\tau}{b-\zeta}\right)^{\frac{1}{2}} + \frac{2}{\pi}\int_{t-1}^{t} g_{tt}(s,t) \ln \frac{[\sqrt{(b-\zeta)(\xi-\tau)}+\sqrt{(\zeta-\tau)(b-\xi)}]^2}{(b-\tau)|\zeta-\xi|} ds, \quad (27)$$

where

$$a_3(t) = \{\int_0^{\tau} q_2(s) + \int_{\tau}^{b} g_t(s,t) - \int_b^{c} q_1(s)\}\left(\frac{\xi}{c-\xi}\right)^{1-\gamma} \frac{d\xi}{|(\xi-b)(\xi-\tau)|^{\frac{1}{2}}}. \quad (28)$$

When the shape function g(s,t) is given, (25), (26) and (27) can be used to calculate the solution of the complete entry.

Special Case as $h \to \infty$

As $h \to \infty$, the problem becomes that of the oblique entry of a fully ventilated foil into a deep ocean. The solutions for the present case may be extracted from those obtained previously by re-scaling the parametric ζ-plane in such a way that point E tends to point D at the point of infinity. This can be achieved by replacing ζ, b, c and τ in the previous solutions by ζ/h, b/h, c/h and τ/h, respectively, and then letting $h \to \infty$. When such a process

is carried out, (11) becomes

$$\frac{\partial z}{\partial \zeta} = -\frac{1}{\pi}\zeta^{-\gamma}(\zeta-b)(\zeta-c)^{\gamma-1}, \tag{29}$$

and (12) and (13) become, respectively,

$$c = b/(1-\gamma) \tag{30}$$

and

$$b = B(\gamma)\pi t, \tag{31}$$

where

$$B(\gamma) = \left(\frac{1-\gamma}{\gamma}\right)^{\gamma}. \tag{32}$$

Similarly, (14) becomes

$$s = \frac{1}{\pi}\int_0^{\xi} \nu^{-\gamma}(b-\nu)(c-\nu)^{\gamma-1}d\nu = tS(\mu), \tag{33}$$

where

$$S(\mu) = B(\gamma)\mu^{1-\gamma}\left(\frac{1}{1-\gamma} - \mu\right)^{\gamma} \tag{34}$$

and

$$\mu = \xi/b. \tag{35}$$

For both the initial and complete entries, the solutions $w(z,t)$, the integral equations which govern $q_1(s)$ and $q_2(s)$, and the pressure distributions on the foil retain formally the same expressions as those shown in the previous sections where the case of finite h was studied, with the exception that the relations (11) to (14) should be replaced by (29), (30), (31) and (33).

A special case for which a closed form solution can be obtained during the initial entry is when $g_t(s,t)$ is given by

$$g_t(s,t) = t^{\beta}s^{\sigma}, \tag{36}$$

where β and σ are arbitrary constants. To seek the closed form

solution, the integral equation (16) is transformed, by using (30), (33) and (35), into

$$\{\int_0^1 g_t(s,t)+\int_1^{\frac{1}{1-\gamma}} q_1(s)\}K(\mu)d\mu = 0, \tag{37}$$

where $K(\mu)$ is given by (19). The substitution of (33) into (36) gives

$$g_t(s,t) = t^{\beta+\sigma}S^{\sigma}(\mu). \tag{38}$$

When (38) is substituted into (37), it becomes obvious that the solution of the integral equation (37) is

$$q_1(s) = -A_{\beta\sigma}s^{\beta+\sigma}. \tag{39}$$

Where $A_{\beta\sigma}$ is a constant,

$$A_{\beta\sigma} = \int_0^1 S^{\sigma}(\mu)K(\mu)d\mu \Big/ \int_1^{\frac{1}{1-\gamma}} S^{\beta+\sigma}(\mu)K(\mu)d\mu. \tag{40}$$

Note that $A_{00}=Q_0(\gamma)$. When the motion of a foil can be expressed as a linear combination of terms of the type shown in (36), the initial entry solution is readily obtainable by the aid of (39). Examples have been given in [1], in which the heaving and pitching motions of a vertically entering flat plate were studied.

After complete entry is achieved, the foil is assumed to move indefinitely into the deep ocean without changing its phase of motion. Eventually, as $t \to \infty$, the flow tends to the classical cavity flow having a zero cavitation number, and no exit phase will occur for this special case. For the case of finite h, the exit phase is considered in the following section.

EXIT

As the leading edge of the foil pierces through the lower free

surface, the layer of water is assumed to be separated into two disconnected flow regions bounded by ATB'EA and DB"CD, respectively, as shown in Fig. 5. In the figure, B' indicates the point of contact between the foil and the lower free surface, and B" the point at which the cavity wall and the lower free surface intersect. All other points in the figure have previously been defined.

To study the hydrodynamic forces acting on the foil during the exit phase, which occurs when $\text{hcsc}\gamma\pi \leq t < \text{hcsc}\gamma\pi+1$, only the flow region bounded by ATB'EA needs to be considered. It should be mentioned here that the entire flow motion from t=0 to $t=\text{hcsc}\gamma\pi+1$ is continuous, since the flow condition at the end of each phase of motion is used as the initial condition for the next phase of motion.

When the linearized approximation is taken, the linearized flow field can be mapped onto the upper-half of a parametric ζ-plane, as shown in Fig. 6, with point A mapped to the origin of the ζ-plane, point E to $\zeta=-1$ and point B' to the point of infinity. The mapping function can be extracted from (11) by letting $b \to \infty$, and the result is

$$\frac{\partial z}{\partial \zeta} = -\frac{h}{\pi} e^{i\gamma\pi} \zeta^{-\gamma} (\zeta+1)^{-1}. \tag{41}$$

The boundary conditions for the present phase of motion may be stated as follows:

$$\phi_\xi = 0 \qquad \text{on } \eta=0^+,\ \xi<0, \tag{42}$$

$$= q_2(s)\left|\frac{\partial z}{\partial \zeta}\right| \qquad \text{on } \eta=0^+,\ 0<\xi<\tau, \tag{43}$$

$$\phi_\eta = g_t(s,t)\left|\frac{\partial z}{\partial \zeta}\right| \qquad \text{on } \eta=0^+,\ \tau<\xi \tag{44}$$

and

$$\phi_\xi = \phi_\eta = 0 \qquad \text{at } \zeta=-1, \tag{45}$$

where s as a function of ξ may be expressed as

$$s = \frac{h}{\pi}\int_0^\xi \xi^{-\gamma}(\xi+1)^{-1}d\xi \tag{46}$$

and τ, again, is the ξ-coordinate of the trailing edge T. As mentioned before, the flow condition at the end of each phase of motion should be used as the initial condition for the next phase. This result is satisfied if $q_2(s)$ in (43), when $s < hcscy\pi-1$, is the solution found at the end of the complete entry.

The boundary-value problem specified by (42) to (45) can be solved, and the solution which satisfies the finite pressure condition at points A, T and B' is

$$w = \frac{1}{\pi}e^{-i\gamma\pi}\zeta^\gamma(\zeta-\tau)^{\frac{1}{2}}\{\int_0^\tau q_2(s)+\int_\tau^\infty g_t(s,t)\}\xi^{-\gamma}|\xi-\tau|^{-\frac{1}{2}}\frac{d\xi}{\xi-\zeta}, \tag{47}$$

subject to the condition that

$$\{\int_0^{t-1} q_2(s)+\int_{t-1}^{hcscy\pi} g_t(s,t)\}|\xi-\tau|^{-\frac{1}{2}}ds = 0, \tag{48}$$

where $0 \le Arg(\zeta-\tau) < 2\pi$ has been chosen.

In (48), $q_2(s)$ is considered as known when $0 \le s < hcscy\pi-1$, and therefore (48) is an integral equation for $q_2(s)$ only when $hcscy\pi-1 \le s < hcscy\pi$. When this part of $q_2(s)$ becomes known, w(z,t) for the exit phase can be determined from (47). However, the asymptotic behavior of w at point B', where $|\zeta|=\infty$, can be visualized directly from (47) without solving (48); the result is that w at B' is bounded if $\gamma < \frac{1}{2}$ and becomes logarithmically singular if $\gamma=\frac{1}{2}$.

An interesting aspect of flow behavior is revealed by studying

the velocity potential f(z,t). When w(z,t) given in (47) is integrated with respect to z, f(z,t) becomes

$$f = f_T - \frac{1}{\pi}\{i\int_0^{t-1} q_2(s) + \int_{t-1}^{hcsc\gamma\pi} g_t(s,t)\}\ln\frac{[\sqrt{\zeta-\tau}+\sqrt{\xi-\tau}]^2}{\xi-\zeta}ds, \qquad (49)$$

where f_T is the value of f(z,t) evaluated at the trailing edge T, ξ is regarded as a function of s and t, and ζ as a function of z and t. The partial differentiation of f with respect to t by holding z fixed yields

$$\frac{\partial f}{\partial t} = -\frac{1}{\pi}\int_{t-1}^{hcsc\gamma\pi} g_{tt}(s,t)\ln\frac{[\sqrt{\zeta-\tau}+\sqrt{\xi-\tau}]^2}{\xi-\zeta}ds + i\{\frac{d\psi_T}{dt} + g_t(t-1,t)\}, \qquad (50)$$

where ψ_T is the stream function evaluated at T. From (50), it is seen that $\phi_t=0$ identically if $g_{tt}=0$. This happens, for example, when the foil is a flat plate. In such a case, the potential ϕ becomes stationary, and therefore the pressure becomes zero throughout the entire flow field. In other words, for a foil whose $g_{tt}=0$ during exit, the flow around the foil becomes conformed to the motion of the foil so that no additional disturbance is generated. To exit, the foil simply slides out of the already established flow without encountering any resistance.

For a general case when $g_{tt}(s,t)\neq 0$, the pressure acting on the wetted part of the foil, which is represented by TB' where $\zeta \geq \tau$, is

$$p = \frac{2}{\pi}\int_{t-1}^{hcsc\gamma\pi} g_{tt}(s,t)\ln\frac{[\sqrt{\zeta-\tau}+\sqrt{\xi-\tau}]^2}{|\xi-\zeta|}ds. \qquad (51)$$

The determination of p does not depend on the solution of the integral equation (48). To determine w(z,t), however, (48) has to be solved.

3. EXAMPLES

Consider a circular-arc foil with a small arc angle 2θ and a small angle of attack α from the entering path. In this case,

$$g(s,t) = (\alpha-\theta)(t-s)+\theta(t-s)^2. \tag{52}$$

This foil degenerates into a flat plate as $\theta \to 0$. When (52) is substituted into (16) and (26), the unknown speed functions $q_1(s)$ and $q_2(s)$ can be solved from the resulting integral equations. The method of solution has been explained in detail in [1]; for convenience, however, it is briefly described in the following.

Since $q_1(s)$ is expected to be bounded everywhere on the cavity wall BC, it may be expanded into a regular series as

$$q_1(s) = \sum_{n=0}^{\infty} b_{mn}(s-s_m)^n \tag{53}$$

for s in the neighborhood of $s=s_m$ (m=0, 1, 2, ...), which is a set of fixed points on the cavity wall BC. The b_{mn} are unknown constants to be determined.

A regular expansion like (53), however, cannot be made for $q_2(s)$ because it is singular at s=0. But, when the singular part is removed, the remainder may be expanded into a regular series. Suppose the singular part of $q_2(s)$ is denoted by $q_2^*(s)$. Then, from (20) and (14), $q_2^*(s)$ may be expressed as

$$q_2^*(s) = -C(1)s^{-(\frac{1}{2}-\gamma)/(1-\gamma)} \quad \text{when } \gamma < \tfrac{1}{2}, \tag{54}$$

where

$$C(t) = \frac{1}{\pi}\left[\frac{h}{\pi(1-\gamma)}\right]^{(\frac{1}{2}-\gamma)/(1-\gamma)} c^{\frac{1}{2}} b^{-\frac{1}{2}\gamma/(1-\gamma)}$$

$$\cdot\left\{\int_0^b g_t(s,t)+\int_b^c q_1(s)\right\}\xi^{-\frac{1}{2}-\gamma}|\xi-b|^{\frac{1}{2}}(c-\xi)^{\gamma-1}d\xi, \tag{55}$$

and as

$$q_2^*(s) = \frac{1}{\pi} g_t(0,1) \ln \frac{s^2}{s^2+1} \quad \text{when } \gamma=\tfrac{1}{2}. \tag{56}$$

Equ. (56) is purposely constructed in such a way that $q_2^*(s)$ tends to zero as $s \to \infty$. It can, therefore, be applied even to the special case when $h \to \infty$. Because the trailing edge of the foil is always one unit above the leading edge, $[q_2(s)-q_2^*(s)]$ may conveniently be expanded into

$$q_2(s)-q_2^*(s) = \sum_{n=0}^{\infty} c_{mn}(s-s_m+1)^n, \tag{57}$$

where c_{mn} are unknown constants.

To study the initial entry phase, (53) is truncated to a polynomial of degree N and substituted in (16). The integral equation is now ready to be solved in steps. Suppose, when m=0, $s_0=t_0=0$ are chosen. Then, (16) contains b_{0n} (n=0, 1, 2, ..., N) as unknown constants. These unknowns can be determined by evaluating (16) at N+1 points in t, starting from the first point at $t=t_0+\delta$, where δ is a small number, and increasing consecutively to the (N+1) point denoted by $t=t_1$, which is assumed to be less than 1. At these points in t the integral equation is satisfied. The resulting N+1 algebraic equations determine the b_{0n}, and therefore $q_1(s)$ becomes known for $0 \leq s \leq t_1$. Since $q_1(s)$ is now known when $0 \leq s \leq t_1$, the portion of the integral equation associated with it may be transfered to the right-hand side of the equation so that the foregoing process may again be used to obtain the solution $q_1(s)$ when $t_1 < s \leq 1$.

Calculations were carried out for a flat plate foil at an angle of attack α and for a circular-arc foil with $\theta=\alpha$. The ad-

vance ratios chosen were $\lambda=0$, 0.5 and 1. In the calculations, the relationship between b and t was determined from (13), which has been shown graphically in Fig. 3. The dependence of s on ξ and t was determined directly from the integral (14). But, for the inverse case when s and t were prescribed, the corresponding ξ was determined from (14) by iterations. As explained before, the iteration process is a straightforward one and can be made to converge for any s on the foil or on the cavity walls. For the initial entry phase, the value of h need not be specified in the calculations, and it is considered a free parameter of the problem.

To study the complete entry, which occurs during the time interval $1 < t < h\csc\gamma\pi$, the integral equations (26) -- instead of (16) -- should be solved. During this phase of motion, $q_2(s)$ is an unknown function in addition to $q_1(s)$ when $s > 1$. When the series expansion (57) for $[q_2(s)-q_2^*(s)]$ is truncated to a polynomial of degree N, the foregoing method of solution may again be used to determine $q_1(s)$ when $1 < s < h\csc\gamma\pi$ and to determine $q_2(s)$ when $0 < s < h\csc\gamma\pi-1$. In the present case, h cannot be considered a free parameter as it was during the initial entry because the value of h is needed in the determination of τ, the ξ-coordinate of the trailing edge of the foil.

The pressure distributions on the foil during the initial and complete entries can be determined from (23) and (27), respectively. Their properties are similar to those shown in [1], where the special case of $\gamma=\frac{1}{2}$ was studied. For illustration, some of the pressure distributions are shown in Fig. 10. The explanation of the

figure will be given at a later stage in this work.

As explained previously, closed form solutions can be obtained for the initial entry phase as $h \to \infty$. When (52) is compared with (36), the solution $q_1(s)$ can easily be obtained by the aid of (39). The result is

$$q_1(s) = -(\alpha-\theta)Q_0(\gamma) - 2\theta Q_1(\gamma)s, \tag{58}$$

where $Q_1(\gamma)=A_{10}-A_{01}$ and $A_{\alpha\beta}$ is defined in (40). The pressure distribution on the foil is

$$p = [(\alpha-\theta)P_0(\gamma)+\theta t P_1(\gamma)][\mu/(1-\mu)]^{\frac{1}{2}} + \theta t G(\mu) \quad \text{for } 0 \le \mu < 1. \tag{59}$$

Where μ is defined in (35),

$$P_0(\gamma) = \frac{2\gamma B(\gamma)}{\pi(1-\gamma)}\left\{\int_0^1 + Q_0(\gamma)\int_1^{\frac{1}{1-\gamma}}\right\}\frac{K(\mu)}{|1-\mu|}\,d\mu, \tag{60}$$

$$P_1(\gamma) = \frac{4\gamma B(\gamma)}{\pi(1-\gamma)}\left\{\int_0^1 [1-S(\mu)] + Q_1(\gamma)\int_1^{\frac{1}{1-\gamma}} S(\mu)\right\}\frac{K(\mu)}{|1-\mu|}\,d\mu \tag{61}$$

and

$$G(\mu) = \frac{4B(\gamma)}{\pi}\int_0^1 [(1-\nu)/\nu]^{\frac{1}{2}}K(\nu)\ln\frac{[\sqrt{\mu(1-\nu)}+\sqrt{\nu(1-\mu)}]^2}{|\mu-\nu|}\,d\nu. \tag{62}$$

The function $G(\mu)$ is always positive when $0 < \mu < 1$ and vanishes when $\mu=0$ or $\mu=1$. Since $0 \le S(\mu) \le 1$ when $0 \le \mu \le 1$, it is not difficult to show that $P_0(\gamma)$ and $P_1(\gamma)$ are positive when $0 < \gamma \le \frac{1}{2}$. This implies that, if $0 < \theta \le \alpha$, the pressure near the leading edge B of the foil is always positive definite during the entire initial entry phase, a condition that will prevent ventilation from developing on the pressure side of the foil. For reference, the function $Q_1(\gamma)$, $P_0(\gamma)$ and $P_1(\gamma)$ are shown graphically in Fig. 7, where the scale for Q_1 is shown on the left-hand side of the figure and that

for P_0 and P_1 on the right-hand side.

When $\theta=0$, the foregoing results correspond to those of a flat plate foil. In this case, p shown in (59) is a function of μ only, i.e., a function of the combined variable s/t only. This means that, as expected, a similarity solution exists for a flat plate during the initial entry when $h=\infty$.

For the complete entry, however, no closed form solution can easily be obtained even for the case of $h=\infty$. The numerical method described previously was used to obtain the solution.

For a finite h, exit occurs during the time interval $h\csc\gamma\pi \leq t < h\csc\gamma\pi+1$. For this phase of motion, the pressure distribution on the foil can be determined directly from (51). In the calculations, the functional relationship between s and ξ was obtained from (46): s was calculated directly from (46) when ξ was given, but ξ was calculated by iterations when s was given. Some of the pressure distributions during the exit phase are shown in Fig. 10.

The force and moment coefficients of the foil are obtained by integrating p, which is defined in (1), over the wetted part of the foil. Suppose the force coefficient in the n-direction, when normalized by the chord length of the foil, is denoted by C_n. Then,

$$C_n = -\int p\,ds. \tag{63}$$

The moment coefficient about the leading edge of the foil, C_{M_B}, may be expressed as

$$C_{M_B} = \int (t-s)p\,ds, \tag{64}$$

where C_{M_B} is positive when the moment is counterclockwise. For the particular type of foils under consideration, the force coef-

ficient in the s-direction, C_s, is related to C_n and C_{M_B} by

$$C_s = (\alpha-\theta)C_n - 2\theta C_{M_B}. \tag{65}$$

Numerical results of C_n and C_{M_B} for a flat plate foil at an angle of attack α are shown in Fig. 8. Fig. 8(a) shows the results of $-C_n/\alpha$ versus t for various values of h. For each value of h, a group of three curves is presented in Fig. 8(a); they correspond to different values of λ, as indicated in the figure. Generally speaking, when other factors are equal, the loading is larger when h is greater, and, within a group of constant h, the loading is larger when λ is larger. Fig. 8(b) shows the corresponding curves for C_{M_B}. For comparison, the force and moment coefficients of the corresponding supercavitating plate, at zero cavitation number, are also shown in Fig. 8(a) and (b) at the location indicated by $t=\infty$. They are the upper bounds of the respective coefficients in the present study.

Since the force (or moment) coefficients for different values of h and λ are nearly equal during the initial entry ($0 < t \leq 1$), they cannot be distinguished clearly in Fig. 8(a) (or 8(b)). For a clearer view, they are plotted in different scales in Fig. 8(c). In reading Fig. 8(c), t should be considered less than, or equal to, unity for any given set of values of h and λ.

Similar results for a circular-arc foil with $\theta=\alpha$ are shown in Fig. 9.

Some representative pressure distributions on the foils are shown in Fig. 10. Fig. 10(a) shows those on the flat plate foil, Fig. 10(b) on the circular-arc foil, and Fig. 10(c) on the circular-arc foil during the exit phase.

The four solid curves shown in Fig. 10(a) indicate the pressure distributions for the case when $h=\infty$ at various times and different values of λ. When the time factor alone is considered, these curves may be divided into two groups: one corresponds to $t=\infty$, and the other to $0 < t \leq 1$, as indicated in the figure. The latter group represents the pressure distributions on the flat plate during the entire initial entry phase ($0 < t \leq 1$) for different values of λ as indicated. The loading is larger when λ is larger. The former group, which consists of a single solid curve, represents the pressure distribution on the plate at any λ when $t=\infty$. This pressure distribution is actually the same as that on the corresponding supercavitating plate at zero cavitation number.

These two groups of curves form the upper and lower bounds for the pressure distributions on a flat plate foil entering an infinitely deep ocean at one of the values of λ considered. In fact, the former group is the upper bound for all possible pressure distributions obtainable in the present study. In conjunction with Fig. 8(a), these two groups are sufficient for visualizing the pressure distributions on a flat plate entering a layer of water of finite thickness.

Suppose, for example, the case of $h=2\pi$ is considered. During the initial entry, the loading on the plate, as shown in Fig. 8(a), is about the same as that for the case of $h=\infty$. This means that, for those values of λ considered, the pressure distributions on the plate during the initial entry are about the same as those shown in the group indicated by $0 < t \leq 1$ in Fig. 10(a). During the complete entry, the loading on the plate, as shown in Fig. 8(a),

increases continuously from that at t=1 until t=3.1, at which time the maximum loading on the plate is about reached. This indicates that during the time interval $1 \leq t \leq 3.1$ the pressure distributions on the plate shift upward from one of the group indicated by $0 < t \leq 1$ shown in Fig. 10(a) to the corresponding one in the group of three broken curves, shown in the same figure, according to the value of λ considered. After t=3.1, the loading on the plate starts to decrease. Therefore, the pressure distributions on the plate start to shift downward from the group of three broken curves shown in Fig. 10(a), and eventually they become identically zero during exit.

For the case when $h=0.5\pi$, the situation is slightly different. From Fig. 8(a), it is seen that the loading on the plate has about reached its maximum at the end of the initial entry phase (t=1). But this maximum loading is less than the loading for the case of $h=\infty$ at t=1. This means that for the case of $h=0.5\pi$ the pressure distributions on the plate for the values of λ considered never exceed those shown in the group indicated by $0 < t \leq 1$ in Fig. 10(a). When t is small, the pressure distributions are about the same as those shown in the group. As t becomes larger, but still less than unity, the pressure distributions over a major part of the plate start to shift downward from those shown in the group except near the trailing edge of the plate, where the pressures may actually shift upward for a while, and eventually all the pressure distributions become identically zero during exit.

For the circular-arc foil, similar situations occur, although the pressure distributions during exit are not identically zero.

Some typical pressure distributions are shown in Fig. 10(b) and (c). Fig. 10(b) is equivalent to Fig. 10(a). Fig. 10(c) shows the pressure distributions on the foil during exit for the case of $h=0.5\pi$. In the figure, ℓ_e indicates the exit length; when $\ell_e=0.01$, for example, it indicates that the leading 1% of the foil has exited from the layer of water. The effect of the thickness of the layer on the pressure distribution during exit is very small. For all three values of h considered ($h/\pi=0.5$, 1 and 2), the pressure distributions are very similar; when λ is constant, their differences do not exceed 1%. Furthermore, it should be noted that those curves shown in Fig. 10(c) are also very similar if both the ordinate and abscissa are normalized by $(1-\ell_e)$. In this case, only three curves, one for each value of λ, are needed to describe the pressure characteristics during exit of the circular-arc foil. Such a similarity, however, may not exist for other foils whose g_{tt} is not constant.

4. CONCLUDING REMARKS

Using the method developed in [1], the problem of oblique entry into and exit from a horizontal layer of water of arbitrary thickness by a two-dimensional, fully ventilated foil has been solved. The present solution contains that obtained in [1]. Therefore, the conclusions derived in [1] are equally valid for the present case. The consideration of oblique entry makes the present solution useful in studying not only the partially submerged supercavitating propeller but also many other problems, such as the high-speed water entry and exit of a wing or a control surface, the operation of a high-speed hydrofoil in a high sea state.

Some prominent features of the present solution are summarized in the following.

When h is infinite and the flow is in the initial entry phase, analytical solutions in series forms can be obtained for arbitrary foil motions, such as heaving and pitching. In other situations, numerical methods are more efficient to effect the solutions.

The velocity at point C (cf. Fig. 1), the intersectional point of the upper free surface of the layer and the cavity wall on the suction side of the foil, is always pointing vertically upward, irrespective of the value of γ so long as $0 < \gamma \leq \frac{1}{2}$. The magnitude of this velocity is equal to $Q_0(\gamma) g_t(0,0) \csc\gamma\pi$.

When $g_{tt}(s,t)$ of a foil is zero during the exit phase, the present linearized theory predicts that the hydrodynamic pressure acting on the foil is zero throughout this phase. This implies that the force characteristics of an exiting foil do not depend on its angle of attack but depend on its camber and its unsteady motions.

From the numerical results obtained in this work, it may be concluded that the effect of the thickness of a layer of water on the force characteristics of a foil entering the layer is not important during both the initial entry phase and the exit phase. However, the thickness of the layer determines the magnitude of the maximum loading on the foil as it goes through the layer. It may also be concluded that, when the angle of attack of a foil measured from the entering path remains constant, the force coefficient $-C_n$ increases as the advance ratio λ increases. Nevertheless, it will never exceed the force coefficient of a corresponding supercavitating foil at zero cavitation number, even when $\lambda \to \infty$ (that is,

$\gamma\pi \to 0^+$).

5. ACKNOWLEDGMENT

This work was supported by the Naval Material Command (0333), Program Element 62543N, Task Area ZF-43-421-001, administered by the David W. Taylor Naval Ship Research and Development Center, Work Unit 1500-200.

6. REFERENCES

1. Wang, D., "Water Entry and Exit of a Fully Ventilated Foil," Journal of Ship Research, Vol. 21, No. 1, 1977, pp. 44-68.

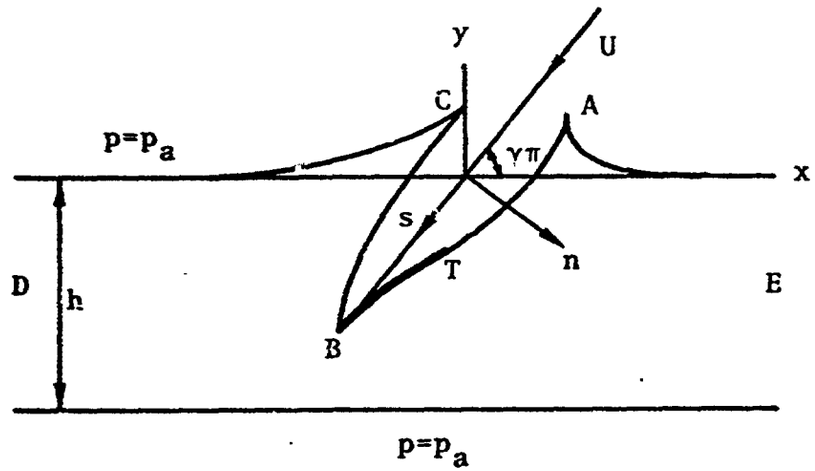

Figure 1. Oblique entry of a fully vented foil into a layer of water of thickness h.

Figure 2. A mapping plane.

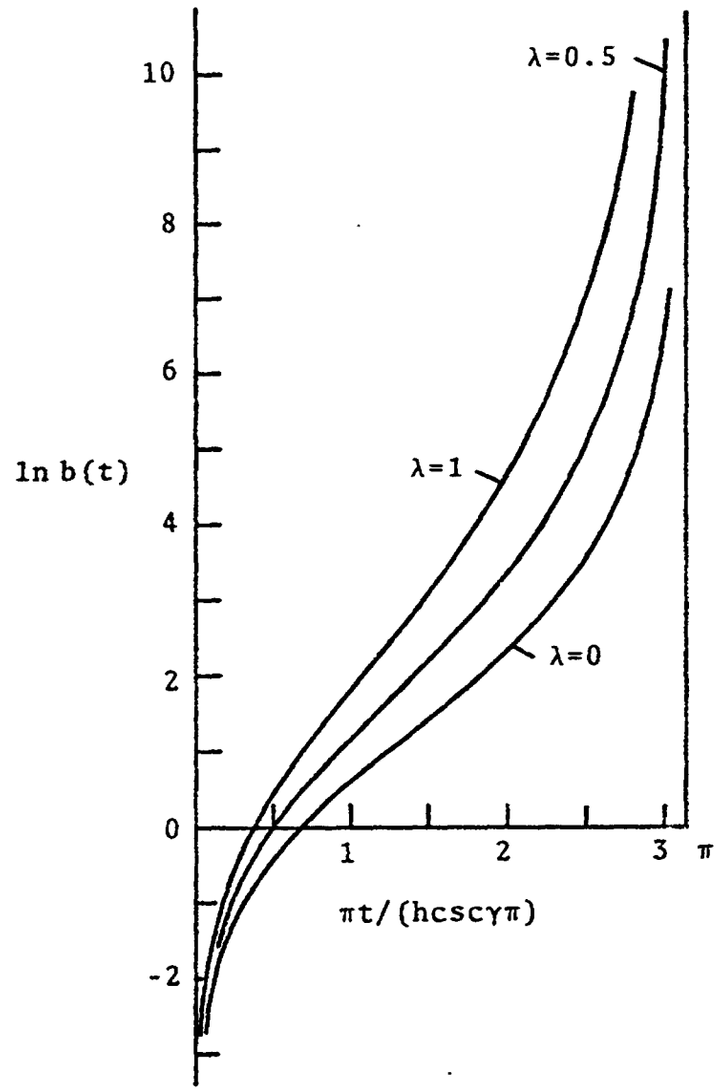

Figure 3. ln b(t) versus πt/(hcscγπ).

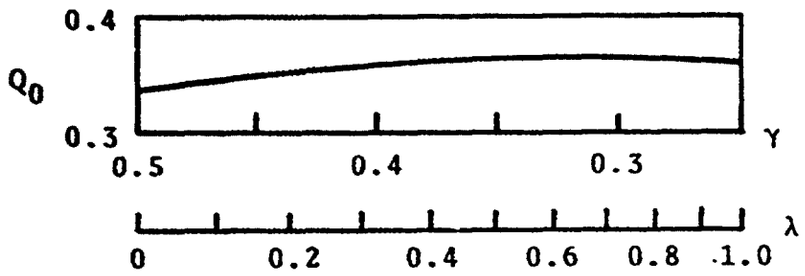

Figure 4. Function $Q_0(\gamma)$.

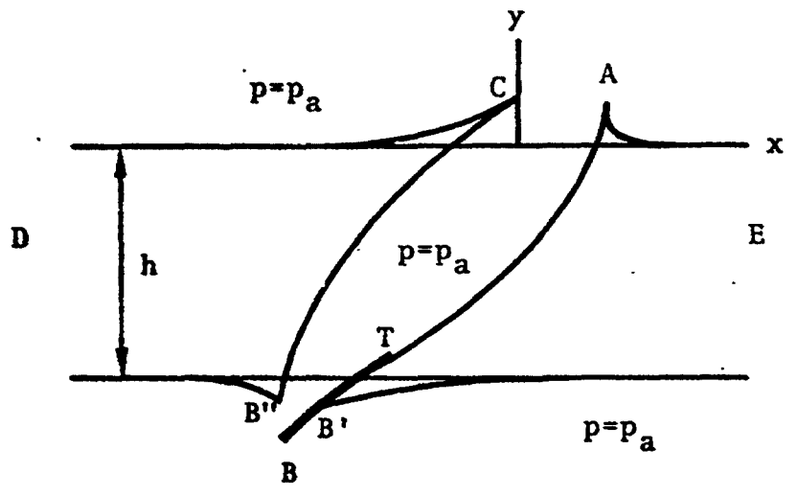

Figure 5. A flow configuration during exit.

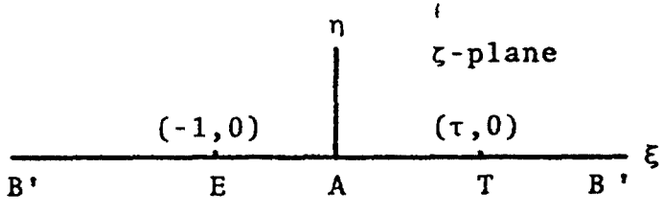

Figure 6. A mapping plane.

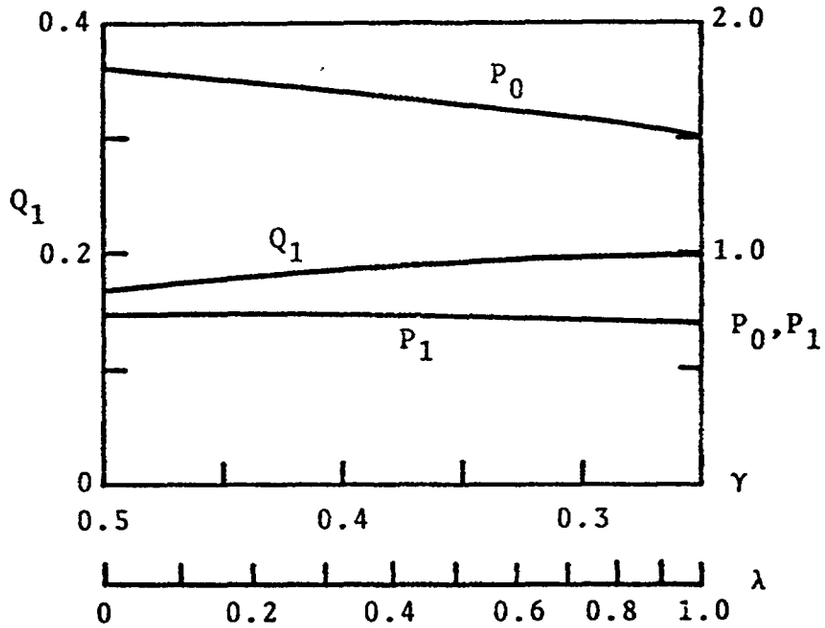

Figure 7. Functions $Q_1(\gamma)$, $P_0(\gamma)$ and $P_1(\gamma)$.

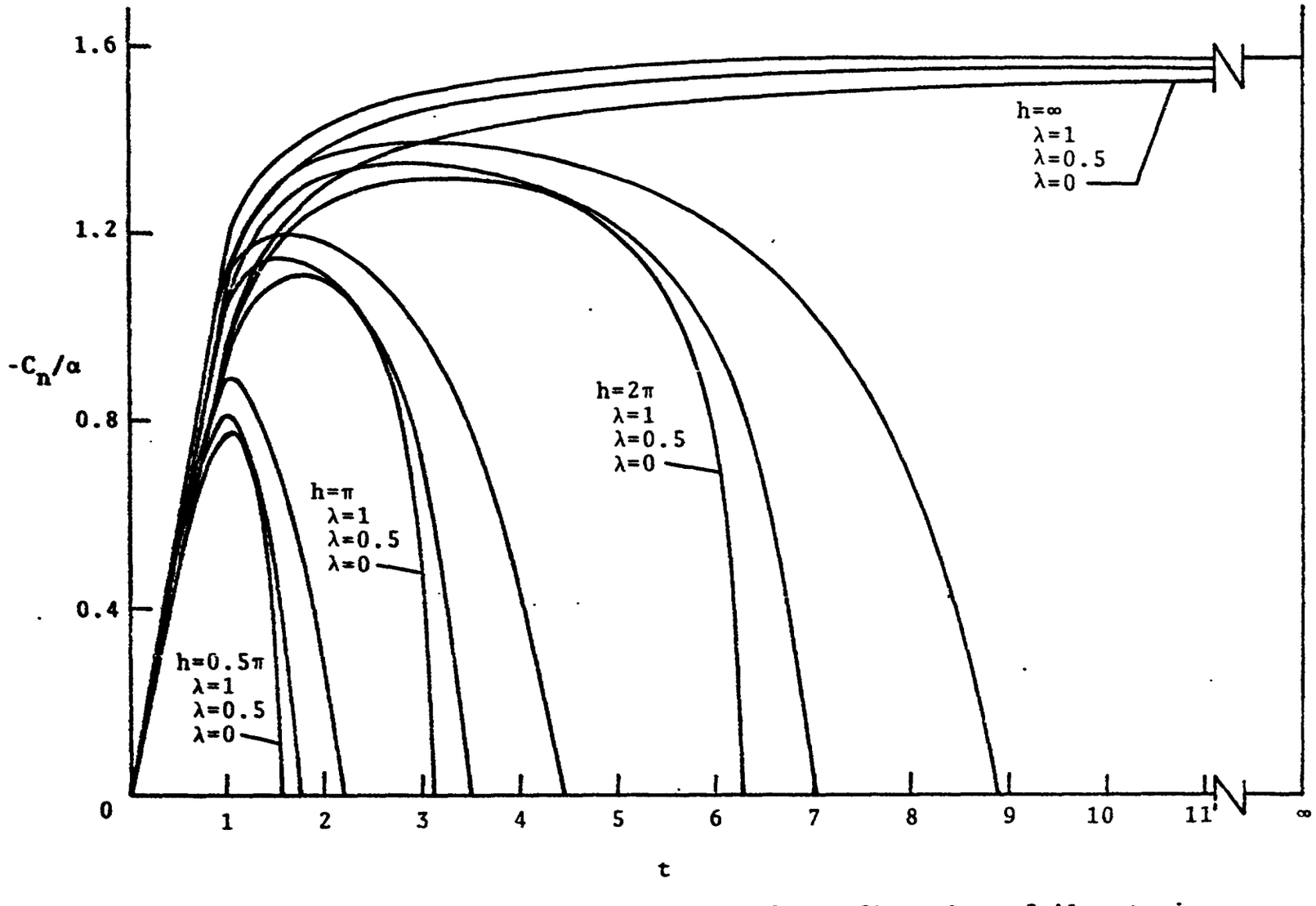

Figure 8(a). Force coefficient versus time for a flat plate foil entering a layer of water of thickness h at several advance ratios.

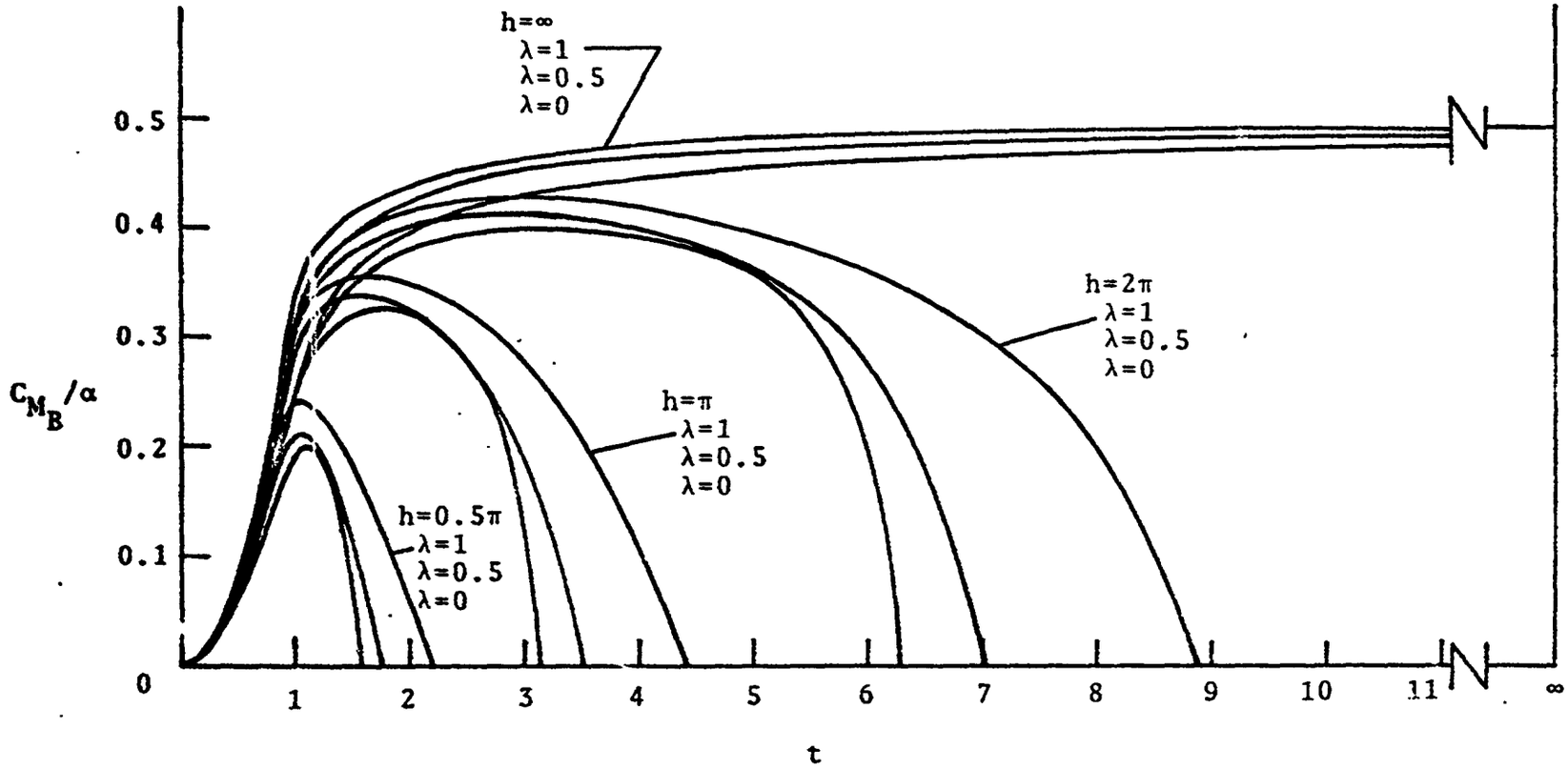

Figure 8(b). Moment coefficient versus time for a flat plate foil.

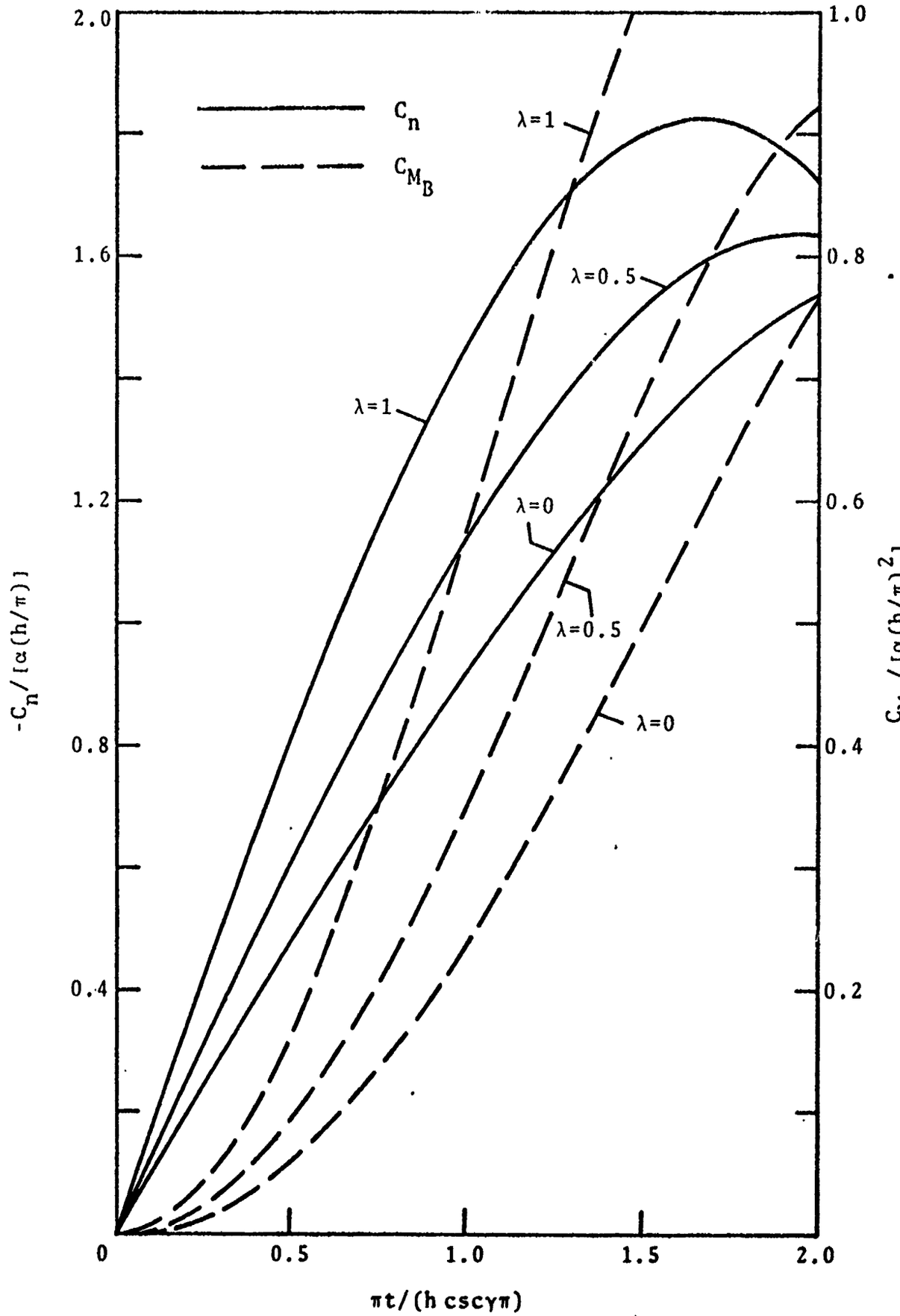

Figure 8(c). Force and moment coefficients versus πt/(hcscγπ) for a flat plate during the initial entry (0<t≤1).

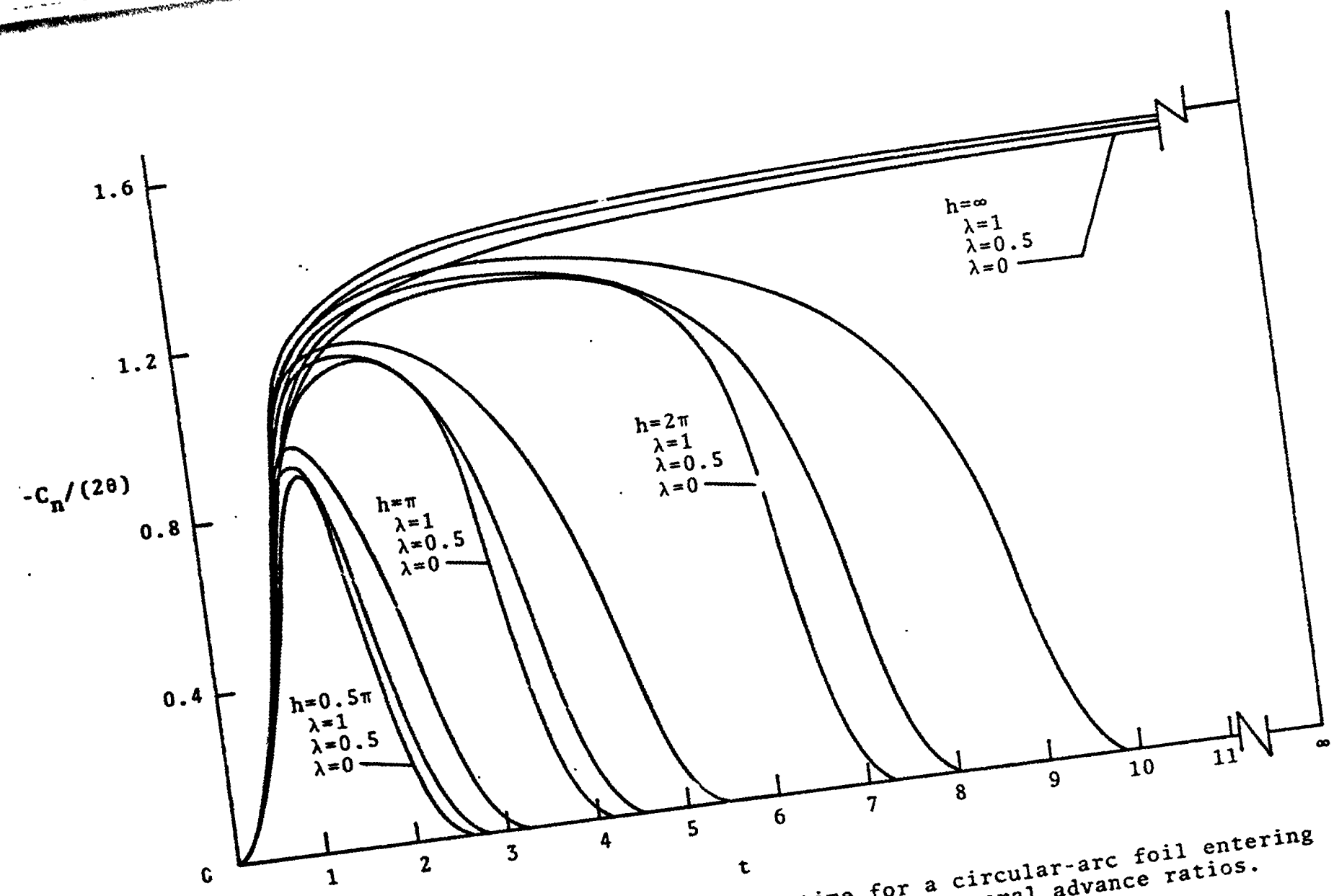

Figure 9(a). Force coefficient versus time for a circular-arc foil entering a layer of water of thickness h at several advance ratios.

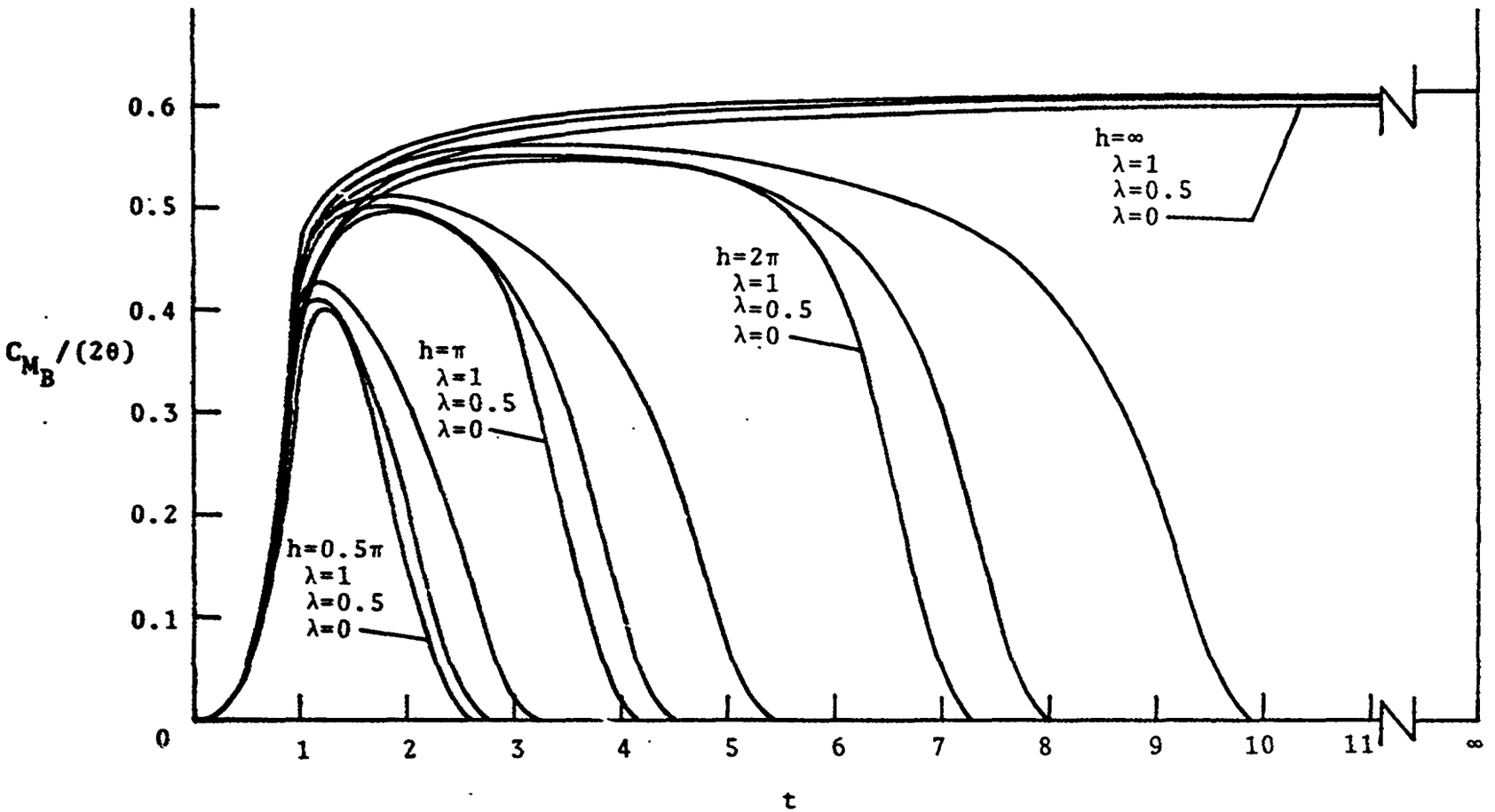

Figure 9(b). Moment coefficient versus time for a circular-arc foil.

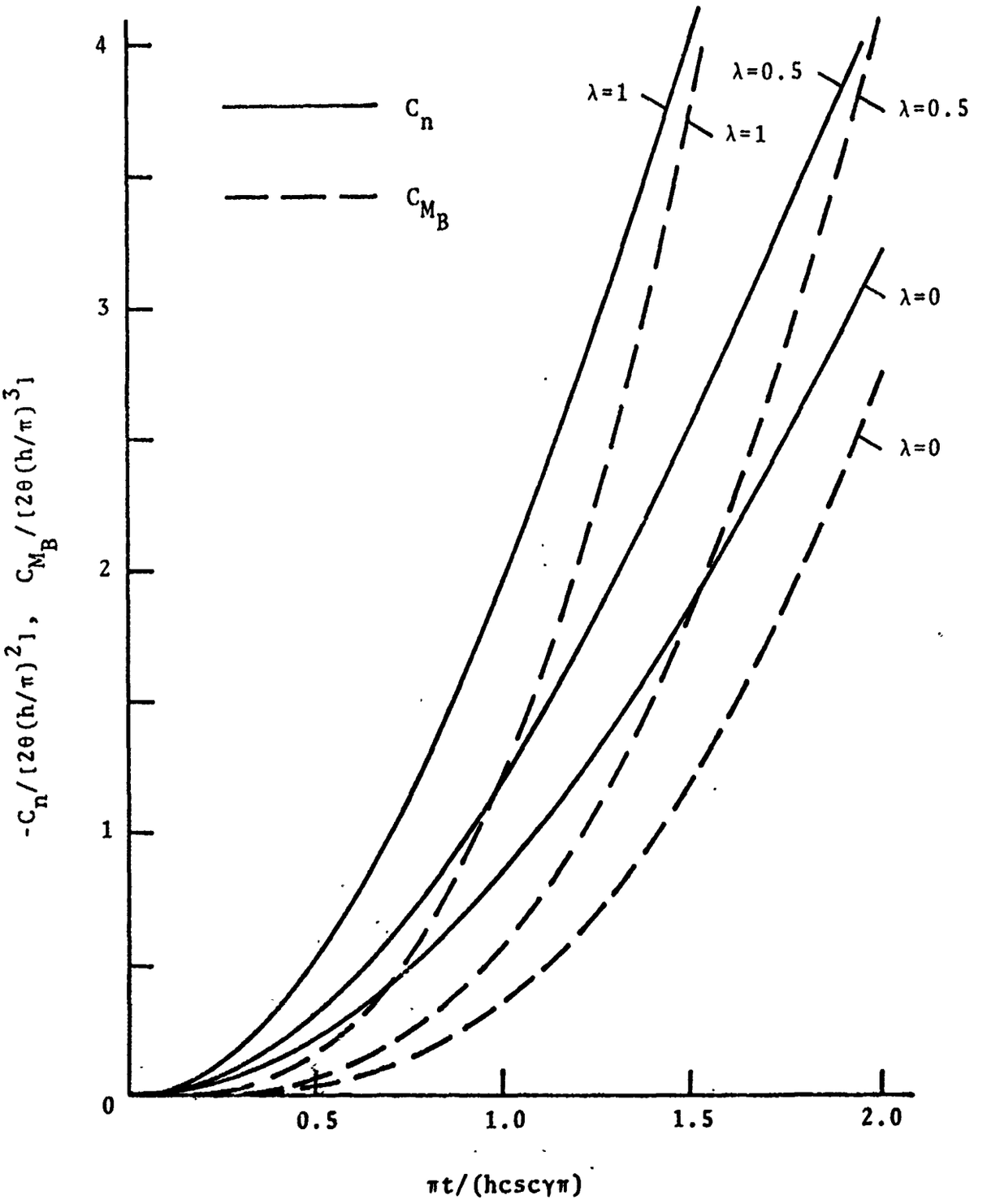

Figure 9(c). Force and moment coefficients versus $\pi t/(h\csc\gamma\pi)$ for a circular-arc foil during the initial entry ($0<t\leq 1$).

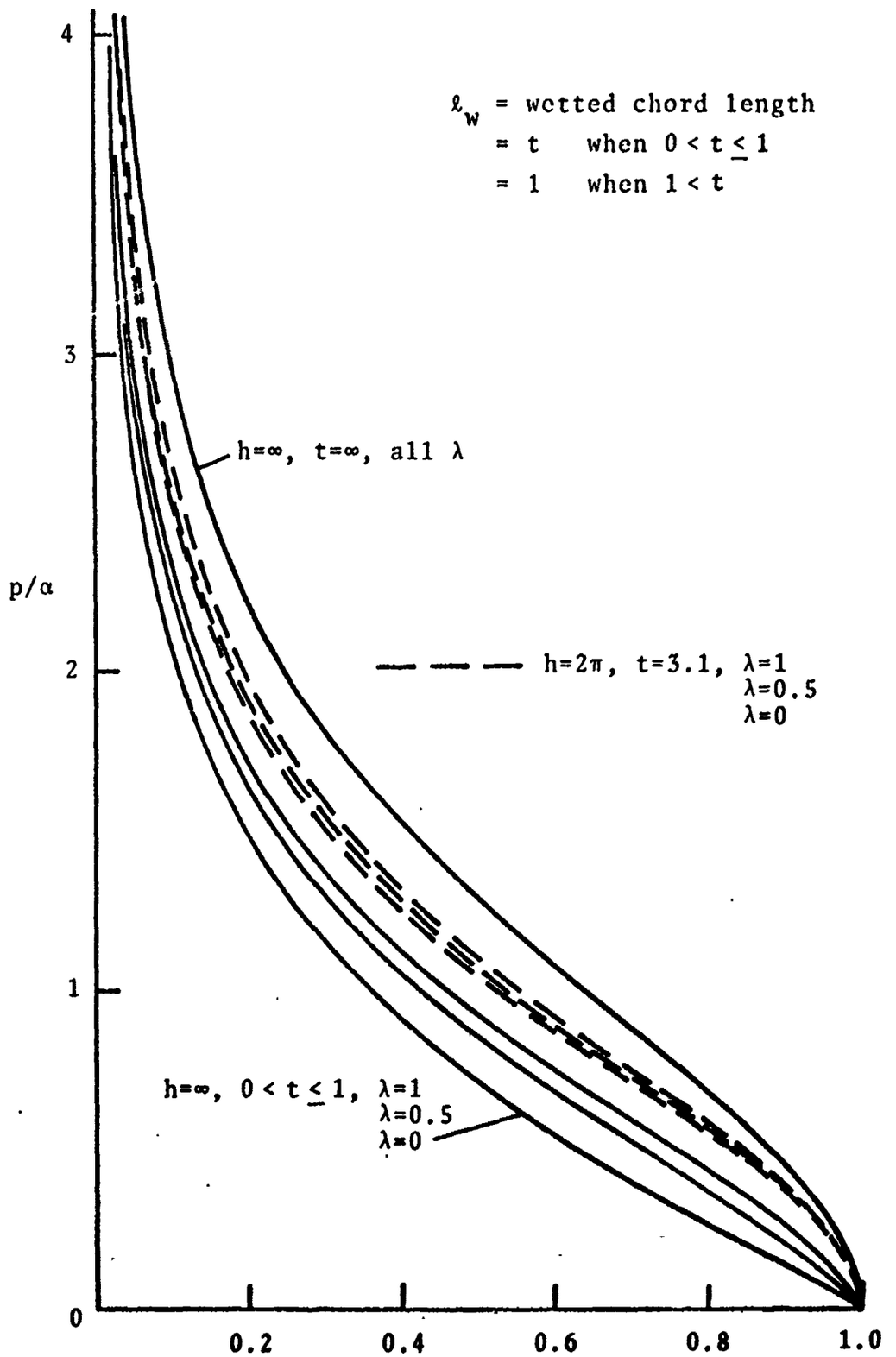

Figure 10(a). Some typical pressure distributions for a flat plate foil.

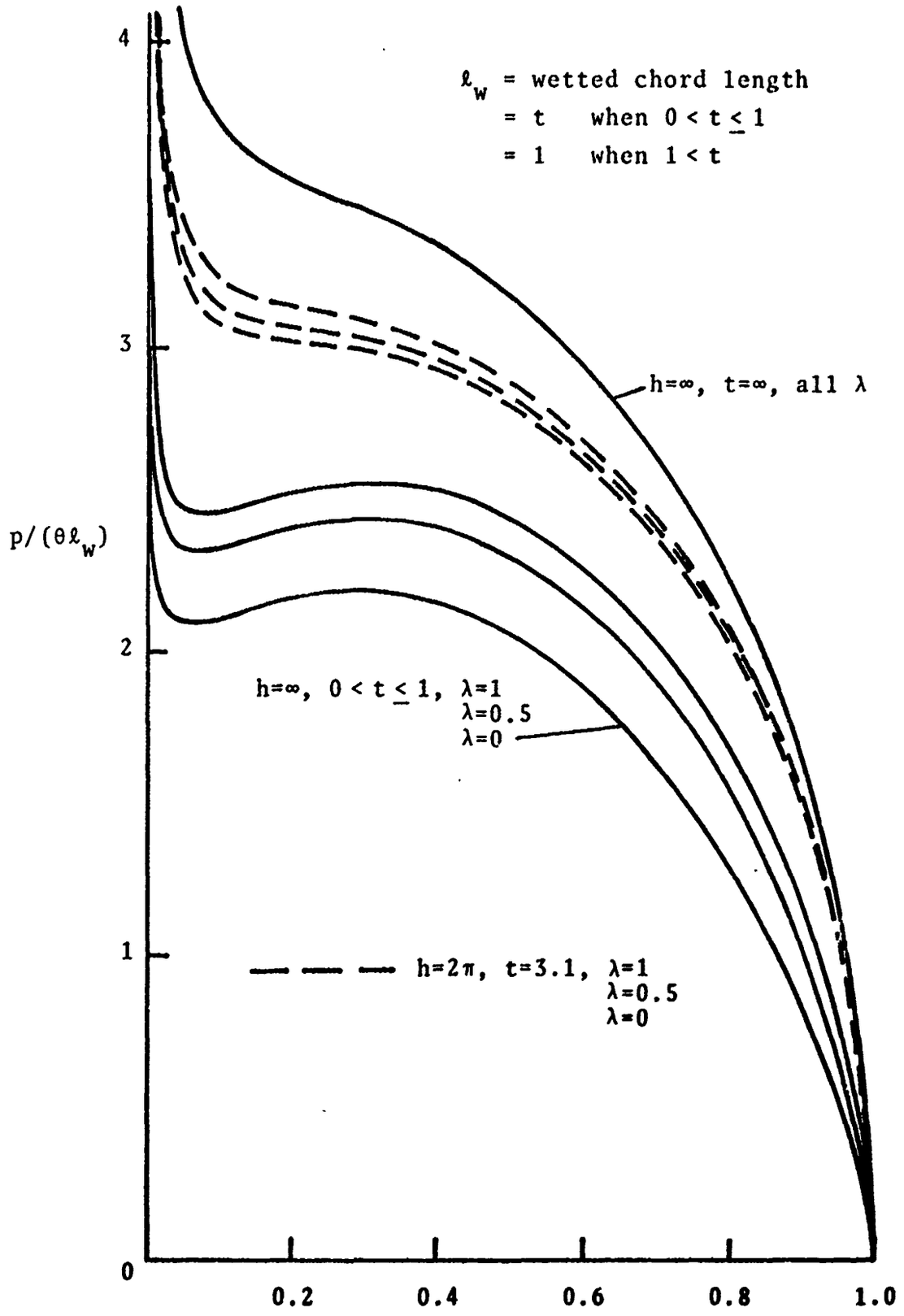

Figure 10(b). Some typical pressure distributions for a circular-arc foil with θ=α.

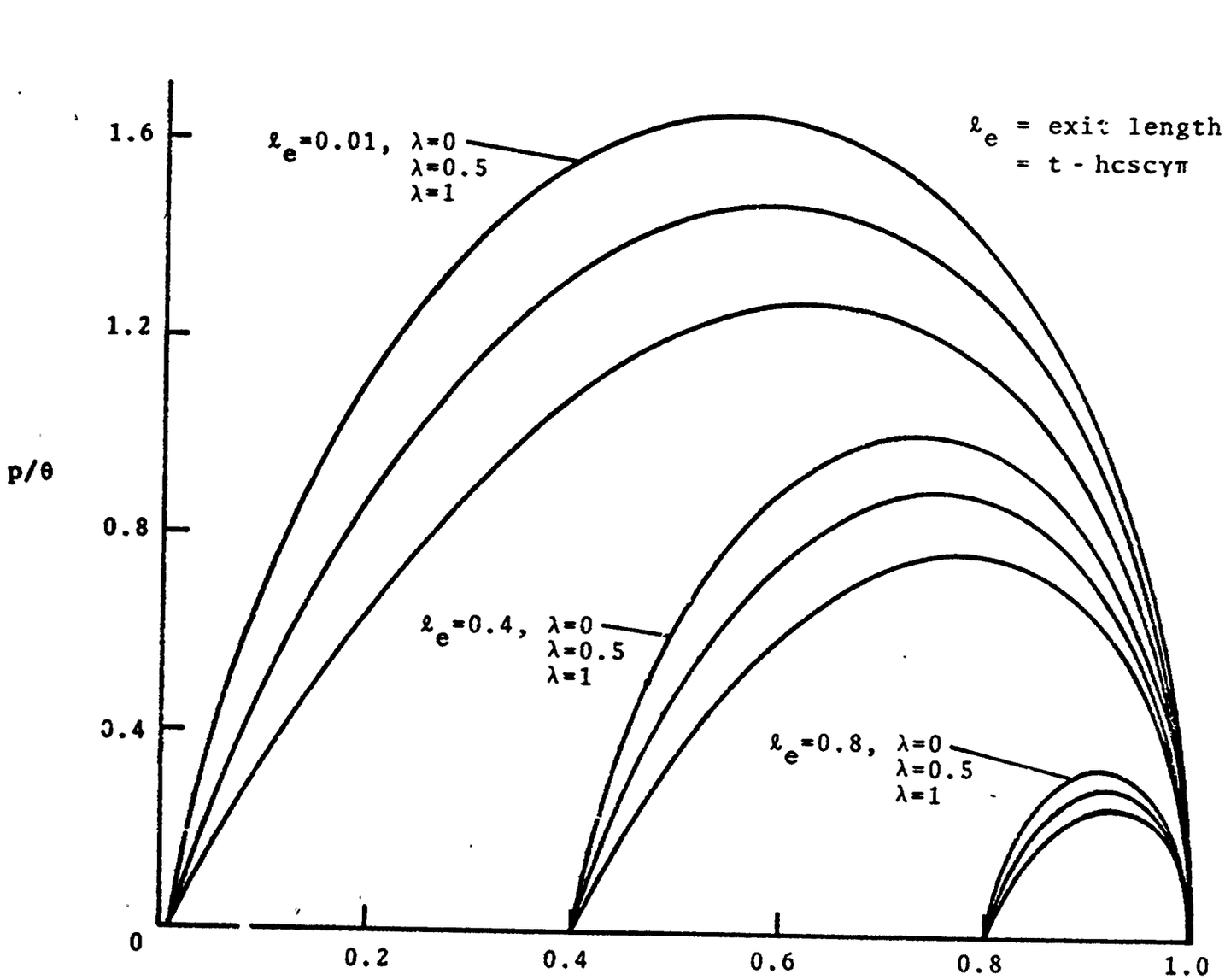

Figure 10(c). Pressure distributions on a circular-arc foil (θ=α) during exit from a layer of water of h=0.5π.